Materials Science and Engineering B 177 (2012) 563–569

Contents lists available at SciVerse ScienceDirect

Materials Science and Engineering B

journal homepage: www.elsevier.com/locate/mseb

Chemical insertion in the perovskite solid solutions $Pr_{0.5+x-y}Li_{0.5-3x}Bi_y\square_{2x}TiO_3$: Implications on the electrical properties

M.F. García-Sánchez[a,*], N. Fernández[b], M.-L. Martínez-Sarrión[c], L. Mestres[c], G. Santana[d], D.W. Lewis[e], A.R. Ruiz-Salvador[f]

[a] Unidad Profesional Interdisciplinaria en Ingeniería y Tecnologías Avanzadas-Instituto Politécnico Nacional (IPN), C.P. 07340, México D.F., Mexico
[b] Departamento de Química Inorgánica, Universidad de la Habana, 10400 Ciudad de la Habana, Cuba
[c] Departament de Química Inorgànica, Universitat de Barcelona, Martí i Franquès 1-11, 08028 Barcelona, Spain
[d] Instituto de Investigaciones en Materiales, Universidad Nacional Autónoma de México, Ciudad Universitaria, Coyoacán 04510, México D.F., Mexico
[e] Department of Chemistry, University College London, 20 Gordon St., London WC1H 0AJ, UK
[f] Instituto de Ciencia y Tecnología de Materiales, Universidad de La Habana, 10400 Ciudad de la Habana, Cuba

ARTICLE INFO

Article history:
Received 4 October 2011
Received in revised form 16 January 2012
Accepted 19 February 2012
Available online 6 March 2012

Keywords:
Lithium ion conductors
Mixed conductors
Chemical insertion
Impedance spectroscopy
Kramers–Kronig relations

ABSTRACT

Chemical insertion and de-insertion of lithium in pellet samples of the solid solutions $Pr_{0.5+x-y}Li_{0.5-3x}Bi_y\square_{2x}TiO_3$ were studied. Two regions of the phase diagram are studied: one having constant composition of bismuth and the other of lithium. The amount of inserted lithium depends on both the number of vacancies and the amount of bismuth in the original samples. The conductivity of the samples is directly related to the amount of inserted lithium and the activation energy depends on the unit cell volume. An analysis of the electronic and ionic components of the conductivity reveals that the untreated materials are pure ionic conductors, while after Li-insertion an additional electronic conductivity ($t < 10^{-2}$) occurs, due to a polaron mechanism, with an activation energy of 0.8 eV.

1. Introduction

Solids with high Li ion conductivity have been subject of increasing attention over the past two decades owing to their application in solid state batteries. With the discovery of the high ionic conductivity of the perovskite $La_{0.51}Li_{0.35}TiO_{2.94}$ at room temperature (10^{-3} S cm^{-1}) [1,2], many studies have sought to identify materials with similar or improved properties [1–13]. For example, materials have been formed through the addition of a rare-earth metal to form $RE_{0.5+x}Li_{0.5-3x}\square_{2x}TiO_3$ (RELTO) materials (where RE and □ denote the rare-earth element and vacancies at the perovskite A-site, respectively) [14], by Li substitution [7,15] and through B-site ion substitution [8]. The reported compounds all show nearly purely ionic conduction with negligible electronic contribution [1–4,8,9,12–16]. Computational studies suggest that the ionic conduction occurs by a percolative motion through 3-dimensional channels connecting the A-site vacancies [17–20]. The structure of these materials has been extensively studied by X-ray diffraction [1–3,5,9,12–15], neutron diffraction [5–7,11,12], transmission electron microscopy [5,6,14], Raman spectroscopy [13,15] and computational simulation [17–20]. But the cation ordering (or the lack of it), as well as mechanism of ion motion through the solid remain topics of some discussion, in part due to the complexity of the materials, but also due to the differences found when materials are prepared under different synthesis conditions. As temperatures in excess of 1300 °C are necessary for the synthesis of these materials, it is known that loss of lithium occurs and, moreover, that different structures can be obtained when different cooling conditions are used [4,8,12]. Chemical methods of synthesis have been used to reduce synthesis temperatures [4,21].

The defect chemistry of this system, i.e. the vacancies and interstitials available for Li^+ cations incorporation and the reducibility of the Ti^{4+}, allows for the insertion of lithium:

$$RE_{0.5+x}Li_{0.5-3x}\square_{2x}Ti^{4+}O_3 + \delta Li^0 \rightarrow RE_{0.5+x}Li_{0.5-3x+\delta}\square_{2x-\delta}Ti_{1-\delta}{}^{4+}Ti_\delta{}^{3+}O_3 \quad (1)$$

Intercalation (also referred as to insertion or lithiation for the particular case of Li) has been reported in TiO_2-based structures [22] and, in particular, in the RELTO system by several groups [12,23–30]. When more lithium ions are inserted than the number of vacant A-sites, it is suggested that insertion also takes place at

* Corresponding author. Tel.: +52 55 5622 4577; fax: +52 55 5616 1251.
E-mail address: rusonil@yahoo.com (M.F. García-Sánchez).

0921-5107/$ – see front matter © 2012 Elsevier B.V. All rights reserved.
doi:10.1016/j.mseb.2012.02.025

3c sites [25,29]. In contrast to non-inserted samples, after lithiation mixed conduction has been reported, although the partition of ionic and electronic conductivities has not been reported [25,26,28]. The electronic conductivity has been explained by the formation of polarons associated with the reduced Ti^{3+} ions [12,26].

Previously, we demonstrated the chemical insertion and de-insertion of lithium in powders of the $Pr_{0.5+x-y}Li_{0.5-3x}Bi_y\square_{2x}TiO_3$ [31]. However, it was not possible to perform electrical measurements on the samples, due to the partial loss of Li during the sintering of the material and which ruled out the possibility to study the relationship between the Li chemical treatment and the electrical behavior.

In this paper, the correlation between the amount of Li and the electrical behavior during chemical insertion and de-insertion of Li in pelleted samples of the $Pr_{0.5+x-y}Li_{0.5-3x}\square_{2x}Bi_yTiO_3$ is investigated. The structural and compositional results are compared with those of Li insertion in powdered samples [31]. A recently developed methodology [32] is used to partition the ionic and electronic contributions to the total conductivity and the role of these distinct mechanisms is discussed in relation to the chemistry of the materials.

2. Experimental and methodology

2.1. Samples preparation

Polycrystalline samples were prepared by solid-state reaction, following a synthetic procedure described in detail elsewhere [31]; here, the account is brief. Pr_6O_{11} (99.9% Fluka), TiO_2 (99.9% Aldrich), Bi_2O_3 (>99% J.T. Baker) and Li_2CO_3 (>99% Merck) were used as starting materials. Pr_6O_{11} and TiO_2 were firstly dried overnight at 900 °C. The reactants were weighed, mixed in an agate mortar with acetone, dried and heated to 650 °C for 2 h to drive off CO_2. After grinding, the samples were pressed (at 2 tons) into pellets of 6 mm diameter and 1 mm thickness, placed in platinum vessels and then covered with powders of the same composition to minimize lithium losses during the thermal treatment [5,21,27,30,31,33]. All pellets were fired at 1100 °C for 12 h giving green products, which were reground, and then pelleted again with the same conditions as before and fired at 1200 °C for another 12 h. A third treatment was carried out at 1250 °C for 4 h for composition IV and 1 h for the other compositions. The longer time for sample IV was necessary due to its lower bismuth content [31].

Since in this system, the highest conductivity is reached within a small portion of the phase diagram [33], and in order to allow comparison with Li insertion in powder samples, here the same five nominal compositions used in the previous work were prepared [31]. These five compositions can be conveniently considered as two groups forming intersecting lines in the composition phase diagram. In samples I, II and III ("line 1"), the lithium and praseodymium composition as well as the number of vacancies change, but the composition of bismuth remained constant (0.04), according to the formula $Pr_{0.46+x}Bi_{0.04}Li_{0.5-3x}\square_{2x}TiO_3$. The second "line" comprises samples II, IV and V, where the number of vacancies and the amount of lithium remain constant (0.20), while the Pr and Bi contents vary to give $Pr_{0.60-y}Bi_yLi_{0.20}\square_{2x}TiO_3$. Nominal compositions of the samples are: (I) $Pr_{0.577}Bi_{0.04}Li_{0.150}TiO_3$, (II) $Pr_{0.560}Bi_{0.04}Li_{0.200}TiO_3$, (III) $Pr_{0.535}Bi_{0.04}Li_{0.275}TiO_3$, (IV) $Pr_{0.590}Bi_{0.01}Li_{0.200}TiO_3$, and (V) $Pr_{0.530}Bi_{0.07}Li_{0.200}TiO_3$.

Crystalline phase identification and lattice parameters were obtained by powder X-ray diffraction, using a Siemens D-500 diffractometer in reflection mode with a graphite monochromator, using Cu-Kα radiation. Lattice parameters were obtained with a silicon internal standard. Li, Bi, Pr and Ti contents were determined by ICP atomic emission spectroscopy using a Thermo Jarrel ASH Corporation, model Spectrometer Polyscan TM 61E.

Chemical lithium insertion was achieved by reacting the pelleted samples with n-BuLi in hexane under a N_2 atmosphere at 80 °C for 3 days with stirring. The de-insertion was carried out by reacting the inserted pelleted samples with I_2 at 80 °C in an acetonitrile solution under a N_2 atmosphere for 3 days with stirring. The amount of n-BuLi and I_2 were in excess (30%) to ensure full insertion and de-insertion, respectively. In both cases, the pellets were washed with the same solvents used for the treatments, prior to chemical and structural analysis. More details of the insertion and de-insertion procedures are described in Ref. [31], as applied to powders of the $Pr_{0.5+x-y}Li_{0.5-3x}Bi_y\square_{2x}TiO_3$.

2.2. Electrical measurements

AC measurements were carried out using an HP 4192A Impedance Analyzer over the range 100 Hz < f < 13 MHz. Both sides of the pellets were polished and painted with gold paste (Engelhard-Clal T-10112) and fired at 900 °C in air to remove the solvent and to gain adhesion. For inserted samples the gold paste was fixed in a furnace with a N_2 atmosphere and heated slowly to 500 °C. Measurements were carried out in the temperature range 25–300 °C at isothermal conditions within an error of ±0.1 °C. At each desired temperature, the samples were equilibrated for 15 min prior to measurement.

Analysis of the conductivity data was carried out by a recently introduced methodology [32], which in a simple way ensures the determination of the ionic and electronic contributions to the total AC conductivity. The methodology is based on the combination of the use of gold electrodes – which do not transport lithium ions – for the electrical measurement and Kramers–Kronig transforms (K–K) during the analysis of the measured data.

The dependence of conductivity with the frequency has the form:

$$\sigma(\omega) = \sigma_{DC} + \varepsilon_o\omega\varepsilon''(\omega) + i\omega\varepsilon_o\varepsilon'(\omega) \quad (2)$$

where σ_{DC} is the frequency-independent conductivity, i.e. the DC conductivity, ε' and ε'' are the real and imaginary part of the dielectric permittivity, respectively. The dielectric permittivity parts are related through the Kramers–Kronig transforms, as follows:

$$\varepsilon'(\omega) = \varepsilon_\infty + \frac{2}{\pi}\int_0^\infty \frac{x\varepsilon''(x)}{x^2-\omega^2}\,dx \quad (3)$$

$$\varepsilon''(\omega) = -\frac{2\omega}{\pi}\int_0^\infty \frac{\varepsilon'(x)}{x^2-\omega^2}\,dx \quad (4)$$

Since DC conductivity does not contribute to the real part of the permittivity (Eq. (2)), it is not included in the χ'' (or ε'') part obtained from χ' (or ε') through the K–K [32,34]: this is quite obvious from a physical point of view, since DC conductivity implies continual flow of charge without energy storage [32,34].

To extract the DC conductivity, the permittivity, ε^*, was calculated from the measured impedance data, according to

$$\varepsilon^* = \frac{1}{i\omega C_o Z^*} \quad (5)$$

where C_o is the vacuum capacitance. Through the use of K–K transforms, the imaginary part of permittivity was calculated from the real part (Eq. (4)). The DC conductivity was calculated as $\sigma_{DC} = \Delta\varepsilon''\omega$, where $\Delta\varepsilon''$ is the difference between the experimental value (ε'') and that calculated ε'' from the real part permittivity curves by the use of the K–K transforms. Note that DC values can be determined for each measured frequency point, and thus one can report a DC value as the average over a large amount of data points

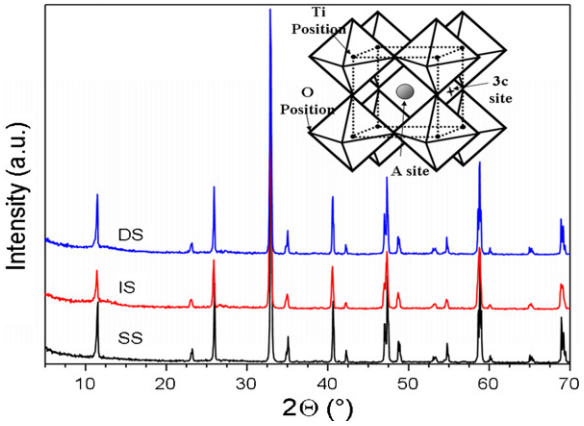

Fig. 1. XRD pattern of starting (SS), inserted (IS) and de-inserted (DS) samples for the composition $Pr_{0.535}Bi_{0.04}Li_{0.275}TiO_3$. In the inset is the perovskite structure indicating the A and 3c sites and the location of the geometric bottleneck between A-sites.

[32,34]. At the same time, by using this procedure one avoids uncertainties introduced by extrapolation of experimental data [9,35] or the use of circuital or mathematical models [36,37].

The K–K transforms were computed using a program reported elsewhere [38], which was written based on the experience of Jonscher and co-workers on the practical implementation of K–K to experimental dielectric data analysis [7,10,21,24,32,33,35,36,39–41]. Impedance spectra were constructed using both the measured data and that obtained from K–K. The resulting spectra were processed by conventional equivalent circuits analysis [7,10,21,24,32,33,35,36,39–41], fitting the data with the Zview software package (Scribner Associates, Inc., Southern Pines, NC). Further details of the whole electrical analysis method can be found in Ref. [32], where its implementation is reported using $Pr_{0.56}Bi_{0.04}Li_{0.2}TiO_3$ as a model material. Here, the results for this compound are also included to allow a complete study of the system.

3. Results and discussion

3.1. Li insertion and deinsertion

For the five compositions studied, the orthorhombic or tetragonal perovskite structure of the non-inserted (as-prepared) samples is retained after Li insertion and deinsertion, as revealed from the X-ray diffraction (XRD) patterns shown in Fig. 1 for sample $Pr_{0.535}Bi_{0.04}Li_{0.275}TiO_3$, as an example. Only slight shifts of the peak positions are observed, which are related to cell expansion and contraction upon variation of Li content, as will be discussed below. In the inset of Fig. 1 the perovskite structure is present, showing the two sites (A and 3c) that have been identified in the literature as host of Li ions [3–6,10–12,17–20]. It is also important to point out that impurity or other phases were not detectable in the XRD patterns of the samples either before or after the Li chemical treatments.

During the insertion procedure a color change [12,22,23,30] from green to black was observed in all the samples, similar to that observed for Li insertion into the equivalent powdered samples [31]. When the pellets were broken, the color inside was uniform indicating, at least qualitatively, that insertion was homogeneous [22]. Results of ICP analyses are shown in Table 1, with the Ti amount set to 1 mole and the remaining values recalculated according to $Pr_{0.5+x-y}Li_{0.5-3x}Bi_y\square_{2x}TiO_3$. The amount of inserted lithium (δ moles of lithium inserted per mole of titanate) and the number of vacancies in nominal composition are also shown to aid discussion. In this paper the number of vacancies in the A-site will be primarily linked to the available sites for Li insertion, as in Ref. [31]. However, it is worth recalling that some structural studies in related materials have suggested that the Li ions are preferentially located at 3c positions (inset in Fig. 1), where the number of vacancies is higher [4,6,7,13,15,19].

It can be observed (Table 1) that for all the compositions prepared the Pr:Bi:Li:Ti ratios were consistent with the values expected from the targeted nominal compositions. Here there is less inserted lithium in the pelleted lithiated samples than in the powdered lithiated samples [31], which is likely to be a result of the smaller surface area of the pellets, compared to the powdered samples: this trend is also found with changing particle size [22].

In the first compositional grouping of samples I, II and III, the amount of lithium inserted is directly related to the increasing number of vacancies: the sites postulated to be those to be occupied by lithium. However, it is interesting to note that the degree of vacancy filling is not consistent, i.e. the ratio of the inserted Li to the number of vacancies varies strongly, from nearly 1 to 0.38 for the higher and lower vacancy contents, respectively. This seems to be caused by multiple factors, including: (i) as the unit cell volume is enlarged, dominated by the increase in the Pr content, the influence of the geometric bottleneck between neighboring A-sites is reduced (i.e. transport is facilitated as the volume of this pathway increases) [13,30,31,33] and (ii) the increase in the number of vacancies increases the 3-dimensional percolation pathways and consequently the accessibility of different sites to the lithium [3,7,9,10,12,13]. It is useful to note that the existence of 3-dimesional pathways in these kind of heavily doped ionic conductors was previously suggested by computational methods [3,7,9,10,12,13].

A comparison of the compositions of IV and V shows that the amount of inserted lithium decreases with increasing bismuth concentration, even though the concentration of vacancies is constant. This must be related to a decrease in lithium mobility caused by the presence of bismuth [33]. All these assumptions are discussed further below along with the results of the electrical measurements.

We now discuss the reversibility of the insertion process, which has been one of the controversial topics in these materials. Here (Table 1) it is found that for each sample the lithium content returns to its initial value following the cycle of insertion and de-insertion of lithium. In other work, García-Sánchez et al. reported that a percentage of lithium is retained when the amount of inserted lithium is higher than the number of A-site vacancies [31]. Birke et al. also showed that intercalation of more lithium than expected for the number of vacancies produces irreversibility in the insertion

Table 1
Pr, Bi and Li content in the starting, inserted and de-inserted samples with general formula $Pr_xBi_yLi_zTiO_3$. The fraction of inserted lithium (δ) and the number of vacancies are also indicated. Calculated uncertainties are indicated in parentheses.

	Experimental starting composition	Inserted lithium composition	De-inserted lithium composition	δ	Number of A-site vac.
I	$Pr_{0.577(4)}Bi_{0.038(2)}Li_{0.159(9)}$	$Pr_{0.574(4)}Bi_{0.038(4)}Li_{0.387(11)}$	$Pr_{0.573(7)}Bi_{0.037(3)}Li_{0.165(13)}$	0.228	0.233
II	$Pr_{0.557(4)}Bi_{0.037(4)}Li_{0.203(6)}$	$Pr_{0.556(5)}Bi_{0.038(4)}Li_{0.323(9)}$	$Pr_{0.558(6)}Bi_{0.038(3)}Li_{0.203(11)}$	0.120	0.200
III	$Pr_{0.533(4)}Bi_{0.038(3)}Li_{0.274(8)}$	$Pr_{0.524(9)}Bi_{0.038(4)}Li_{0.331(7)}$	$Pr_{0.533(6)}Bi_{0.038(2)}Li_{0.288(12)}$	0.057	0.150
IV	$Pr_{0.579(6)}Bi_{0.011(1)}Li_{0.224(12)}$	$Pr_{0.583(7)}Bi_{0.011(2)}Li_{0.398(9)}$	$Pr_{0.580(9)}Bi_{0.011(1)}Li_{0.231(9)}$	0.174	0.200
V	$Pr_{0.526(8)}Bi_{0.066(4)}Li_{0.214(11)}$	$Pr_{0.534(5)}Bi_{0.067(3)}Li_{0.320(8)}$	$Pr_{0.523(7)}Bi_{0.068(3)}Li_{0.214(6)}$	0.106	0.200

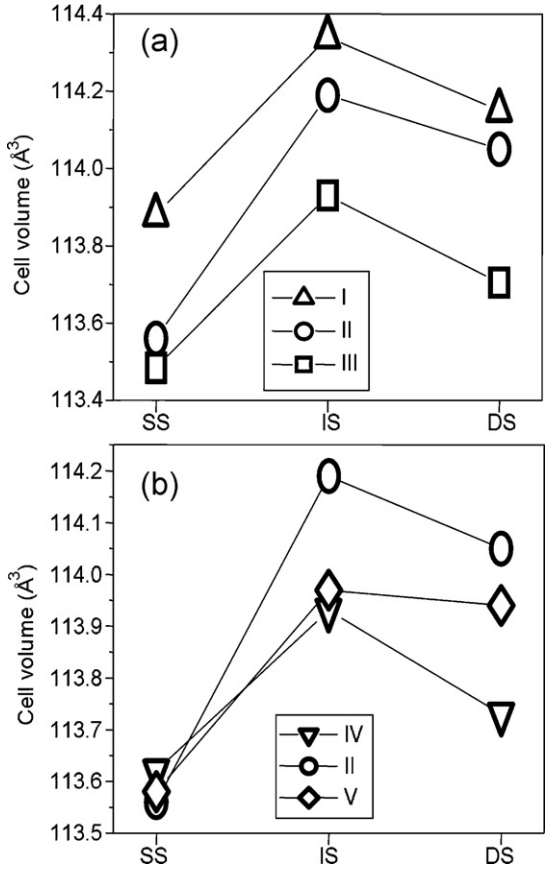

Fig. 2. Unit cell volume in the starting (SS), inserted (IS) and de-inserted (DS) samples for the two compositional groupings.

process, manifested by a change in the titration curve [23], which they attributed to the formation of a second solid phase, although no XRD data were reported. Shan et al. suggested that lithium ions are inserted in A-site vacancies until these are fully occupied and that the remaining fraction then inserts into 3c-site positions, with a larger increase in cell volume [28]. Of course, such a mechanism results in a change in the distribution of Li ions within the lattice. Recent computational simulations showed that not all A-sites are energetically equivalent, which is related to the Li distribution, and suggested the occurrence of trapping regions around some specific positions for the lithium ions hopping within the crystal structure [17]. The occupation of these trapping regions must be favored when the amount of inserted lithium is higher. Based on the above results, we speculate below about the maximum amount of inserted lithium that permits the reversibility of the insertion process, which can be used to explain the discrepancies reported [23–29,31].

Fig. 2 shows the unit cell volume of the starting solids, lithium inserted and de-inserted samples and the calculated volume values are reported in the supplementary material. The unit cell volume of the orthorhombic structures has been divided by two to facilitate comparison with previous work [31,33]. As expected, lithium insertion is accompanied by an increase in the unit cell volume, but after de-insertion the volume still remains higher than those of the starting samples. This behavior could be related to trapped Li ions [17] and in order to understand this behavior, a combined crystallographic and computational study is underway. However, what is currently clear is that despite the fact that the bulk Li content returns to the original composition, the insertion/de-insertion process cannot be considered as reversible, in agreement with the conclusion achieved by Birke et al. from the behavior of the titration curves [23].

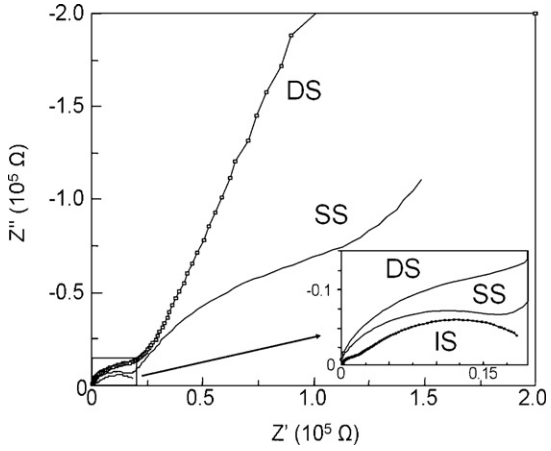

Fig. 3. Plots of Z'' vs. Z' for composition V ($Pr_{0.530}Bi_{0.07}Li_{0.200}TiO_3$) measured at 110 °C. The response of the starting (SS), inserted (IS), and de-inserted (DS) samples are shown in the same plot. Inset is an enlargement of the high-frequency portion of the main figure.

3.2. Impedance response of the starting, inserted and deinserted samples

The general appearance of the complex impedance spectra of the starting and de-inserted samples are two semicircles and a spike, while the spike is not found in the spectra of the inserted samples. This behavior is illustrated for sample V (Fig. 3), using the data taken at 110 °C because at this temperature it is possible to see the impedance response arising from the electrodes, grain boundaries and grains. The appearance of the spike (and not the beginning of a new semicircle) is associated with the absence of a long range conducting path which results in a polarization effect in the material [32]. In the present case, since the gold electrodes block the flow of the lithium ions, an interfacial polarization effect is developed at the material-electrode surfaces [12,26,31,33]. The fact that the spike is not detected in the inserted samples is evidence that the gold electrodes are not blocking, at least partially, the current flow which suggests a high electronic mobility upon Li insertion in these materials. Such a change can be considered a result of the partial reduction of Ti^{4+} to Ti^{3+} during insertion [12,26].

The equivalent circuit used for modeling the impedance spectra of inserted samples is composed of two blocks formed of parallel R-C-CPE (constant phase element) elements which are themselves joined in series [16,41]. It is important to note that, at this stage, we are not making a distinction (through the use of this equivalent circuit) between single (ionic or electronic) and mixed electrical (ionic + electronic) behavior. Another CPE in series was added for fitting the response of the spike in the starting and de-inserted compositions [31,33]. The suitability of the use of CPEs is an indication of the presence of non-Debye processes, typical of ionic conductors [10,16,24,31,33,36,39,41]. The fitting of the first and second semicircles in all samples showed capacitances of around 0.4 pF and 3 nF, which suggests that they are related to processes in the bulk and at grain boundaries, respectively [39]. The spike has a capacitance of 30–60 nF, which suggests a dielectric layer at the pellet surface [33]. Arrhenius plots were processed for the bulk conductivity values obtained from the equivalent circuit processing at different temperatures: good fits were obtained in all cases. Conductivities at 25 °C and the resulting calculated activation energies for each sample are given in Table 2.

Table 2
Bulk conductivity at 25 °C and activation energy of the starting, inserted and de-inserted samples. Calculated uncertainties are indicated in parentheses.

	Starting sample		Inserted sample		Deinserted sample	
	σ $(\Omega\,cm)^{-1}$	E_a (eV)	σ $(\Omega\,cm)^{-1}$	E_a (eV)	σ $(\Omega\,cm)^{-1}$	E_a (eV)
I	$5.63(8)\times10^{-6}$	0.404(6)	$1.76(3)\times10^{-4}$	0.374(6)	$4.50(8)\times10^{-6}$	0.409(7)
II	$4.41(9)\times10^{-6}$	0.441(7)	$9.07(13)\times10^{-6}$	0.379(6)	$2.90(6)\times10^{-6}$	0.416(8)
III	$3.57(7)\times10^{-6}$	0.455(6)	$7.43(11)\times10^{-6}$	0.382(7)	$2.49(6)\times10^{-6}$	0.437(8)
IV	$6.74(9)\times10^{-6}$	0.391(6)	$6.94(9)\times10^{-5}$	0.324(6)	$4.50(9)\times10^{-6}$	0.354(7)
V	$5.93(9)\times10^{-6}$	0.454(8)	$1.43(3)\times10^{-5}$	0.434(7)	$6.50(9)\times10^{-6}$	0.436(9)

In the starting samples, the bulk conductivity is of the same order for all compositions. Differences are due to the complex interplay between the number of charge carriers (Li^+ ions), activation energy and the mobility correlation factor. Upon insertion, the conductivity increases by a factor of ~2 in samples II, III and V, while in samples I and IV it is increased by a factor of around 20 and 10 times, respectively. These latter two samples are those which have the higher levels of Li insertion (Table 1). During de-insertion the conductivity decreases back to values slightly lower than those of the original starting materials. This drop in the conductivity is an unexpected finding since both the Li content (Table 1) and the unit cell volumes (Fig. 2) of the de-inserted samples remain slightly larger than the respective values of the starting materials. However, such a result can be rationalized by noting that after insertion a fraction of the Li ions enter and remain in 3c sites, as was suggested above from the analysis of the cell volumes.

Fig. 4 shows the variation of activation energy of both groups of compositions for each sample form (starting, inserted and de-inserted). The activation energy is more directly related to structural parameters such as cell volume or distributions of cations, than to the conductivity that is also affected by the number of charge carriers and the mobility correlation factor. An increase in unit cell volume results in a decrease in the activation energy as the bottleneck between A sites is diminished [3,6,12,31]. There should therefore be a direct correlation between the cell volume (Fig. 2) and the activation energy (Fig. 4). As the Li and Pr content changes in the grouping of samples I, II and III, the activation energy decreases after insertion due to the increase in unit cell volume (Fig. 4a). The activation energy is slightly lower in de-inserted samples than in starting samples, as the unit cell volume of these samples does not return to that of the original materials. For samples IV, II and V where the lithium content is constant, there is a relationship between the activation energy and the concentration of bismuth (Fig. 4b). This could be related to the high polarizability of bismuth, as previously reported [31,33] and may therefore be the cause of the reduction in the amount of lithium that can be incorporated when the concentration of bismuth increases.

As suggested, the inserted samples are likely to have mixed (electronic and ionic) conduction. Emery et al. suggest that, in related materials, electronic conduction is through a polaron-mediated mechanism [26]. Polarons are created when electrons polarize their surroundings leading to localized states with low mobility. The activation energy for this mechanism will depend mainly on the transfer of electrons from Ti^{3+} to Ti^{4+} and must be constant during the insertion. Here, however, the values of the activation energy correlate with the variation of the amount of inserted lithium and the unit cell volume, which suggests that the AC electrical response is dominated by the contribution from ionic conductivity. Therefore, the electronic conductivity must be a much smaller contributor, although the absence of a spike in the response proves its presence in the total response, which is in agreement with observations in similar materials at $T > 127$ °C [28]. Thus, the relative magnitude of the ionic and electronic components is now evaluated, following the methodology developed in Ref. [32].

3.3. Analysis of DC component

Our results show that σ_{DC} is independent of frequency, i.e. a constant value for all frequency points, and characterizes the material as a whole and is not associated to the conductivity of any specific microregion of the material. That is, it cannot be associated with the usual microregion (bulk, grain boundary or electrode) conductivity determined by equivalent circuit analysis of the impedance spectra. Details of the processing model and its application to composition II are shown in Ref. [32].

The values of the DC conductivity (when it could be calculated) and activation energies are given in Table 3. As expected, the DC conductivities of starting and de-inserted samples are extremely low. These values are lower than those obtained from DC measurements in lithium lanthanum titanates (LLTO) samples [26]. The uncertainty in the calculated values is high as these values are at

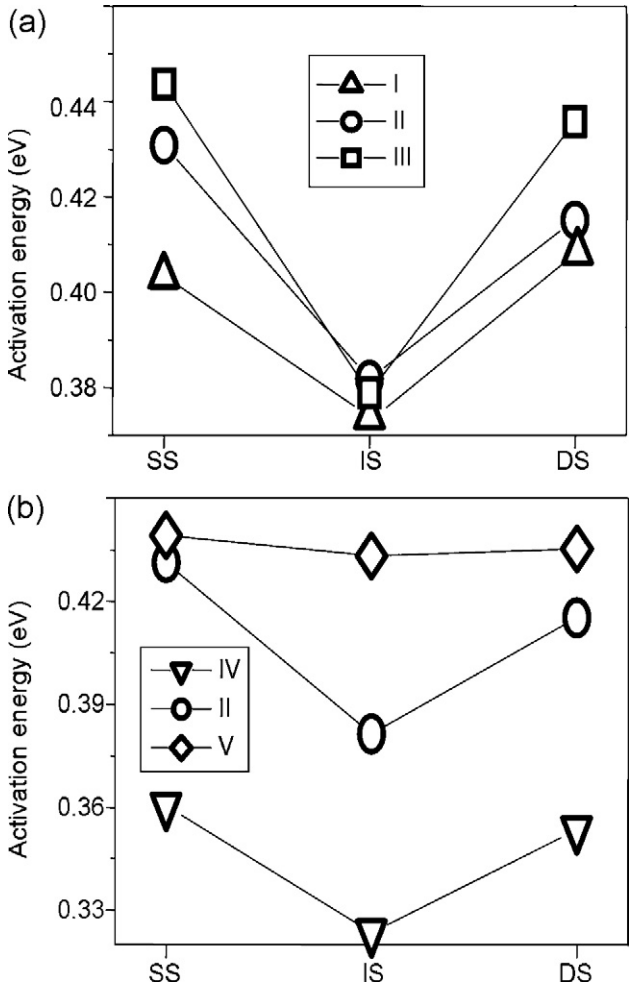

Fig. 4. Activation energies for conduction (eV) of the starting (SS), inserted (IS) and de-inserted (DS) samples for the two compositional groupings.

Table 3
DC conductivity at 25 °C and the activation energy of starting, inserted and de-inserted compositions. Calculated uncertainties are indicated in parentheses.

	Starting sample		Inserted sample		Deinserted sample	
	σ (Ω cm)$^{-1}$	E_a (eV)	σ (Ω cm)$^{-1}$	E_a (eV)	σ (Ω cm)$^{-1}$	E_a (eV)
I	$1.7(4)\times10^{-12}$	0.81(17)	$2.75(2)\times10^{-6}$	0.84(3)	$9.8(1.3)\times10^{-12}$	0.67(22)
II	$1.7(2)\times10^{-11}$	0.73(11)	$3.28(2)\times10^{-10}$	0.84(3)	$9.8(1.2)\times10^{-13}$	0.83(14)
III	$1.4(3)\times10^{-12}$	0.89(19)	$5.03(5)\times10^{-10}$	0.74(6)	$2.1(9)\times10^{-12}$	0.81(33)
IV	$7.8(4)\times10^{-12}$	0.77(18)	$8.77(6)\times10^{-6}$	0.77(4)	$4.2(1.1)\times10^{-13}$	0.98(23)
V	$1.7(6)\times10^{-13}$	0.95(27)	$2.71(4)\times10^{-9}$	0.87(5)	–	–

the lower limit of this method and numerical errors can arise in the calculations. For instance it was not possible to determine the DC values because of the extremely low sigma values. However, despite these uncertainties, it can be observed that the electronic transport number ($t=\sigma_{electronic}/\sigma_{ionic}$) is lower than 10^{-5}, which is of the same order as reported for the LLTO system [12]. Thus, it can be concluded that conduction in the original and de-inserted samples can be considered as purely ionic. However, in the inserted samples, a significant increase is observed in the DC conductivity, correlated to the amount of inserted lithium. When higher levels of lithium are inserted (samples I and IV), the increase in DC conductivity is larger, indicating a higher number of electrons. Such an increase is consistent with a contribution to the conductivity via polarons. As more lithium is inserted, more titanium is reduced and hence the number of conduction pathways and carriers available increases, resulting in a higher conductivity.

For the inserted samples, within the error bars, the activation energy is almost constant at about 0.8 eV. For the starting and deinserted samples the error bars are much larger, but one can visualize that within these limits the activation energy is also about 0.8 eV. This would suggest that the mechanism of electronic conduction do not differ between the insertion and de-insertion processes. The values of the activation energy obtained are similar to that obtained (0.75 eV) when TiO_2 crystals are reduced, which provide further evidence for the electronic conduction mechanism proposed [42]. These results are also in agreement with the polaron formation suggested from ^{7}Li NMR experiments [12,26]. Then, the changes in the DC conductivity are mainly due to the variations in the number of charge carriers during insertion, as was discussed.

The goodness of the fit in the Arrhenius plots for the conductivities [32] and the large difference between E_a values for both electronic and total conduction, strongly suggests that the mechanisms are independent, as previously suggested by Emery et al. using NMR relaxation in similar materials [26]. In order to determine the grain DC ionic conductivity of the inserted samples, the measured data were again processed using K–K transformations. Since the electronic conductivity is present in the overall DC data (Table 3), the application of the K–K to the real component of the permittivity now gives the imaginary part with no DC component. Thus, in this way, the contribution from the electronic conductivity is removed while keeping that which is ionic in nature. After the transformations, the impedance spectra resulted in two semicircles and one spike, similar to that already obtained for the starting and de-inserted samples. Fitting these impedance data, the grain conductivity values at 25 °C and the activation energy were calculated (Table 4). The errors shown in the tables contain both the instrumental and simulation errors, which are much larger than those of the mathematical processing used here.

When comparing the values for the inserted samples in Table 2 with those in Table 4 one should note that in Table 2 both electronic and ionic contributions are present and their values have been calculated as effective conductivities without partition between ionic and electronic, while in Table 4 only the ionic component of the grains is present. It is important to note that the method used here to determine the pure ionic conductivity cannot be substituted by a simple subtraction of the electronic conductivity values (Table 3) from those in Table 2.

Table 4
Grain ionic conductivity at 25 °C and the activation energy of bulk of inserted compositions. Calculated uncertainties are indicated in parentheses.

	Inserted sample with electronic DC component removed	
	σ (Ω cm)$^{-1}$	E_a (eV)
I	$1.02(12)\times10^{-4}$	0.35(3)
II	$3.38(14)\times10^{-6}$	0.38(4)
III	$8.2(8)\times10^{-6}$	0.36(4)
IV	$2.30(21)\times10^{-5}$	0.30(3)
V	$1.36(15)\times10^{-5}$	0.43(4)

The analysis of the grain ionic conductivity (Table 4) indicates that the behavior is similar to that discussed above for the starting and de-inserted samples. The activation energy decreases as more lithium is inserted as consequence of changes in unit cell parameters and the conductivity increases with the number of carriers. It is now more evident that the ionic conductivity dominates in the total electrical response of the materials. The correlation of the dependence of the conductivity with the availability of vacant A sites – the number of vacant A sites in the inserted samples minus the number of inserted Li – reveals that interstitial 3c sites are key to the ionic conduction in these solids. However, whether these sites are associated with alternate conduction pathways or act only as temporary residential sites for Li cations cannot be determined for this present work.

It should be noted that, although general and complex equivalent circuits have been developed for mixed conductors [40], the present method gives an unambiguous and confident calculation of the electronic component without recourse to any previous model and has a clear physical basis [32]. Thus the goal of the analysis methodology used here, being not only the calculation of the DC conductivity with high precision but also to establish the contribution of the ionic and electronic conductivities and their individual activation energies, is achieved. Establishing the DC conductivity is essential in the application of these materials, while the latter provides insight into the microscopic origin of the conductivity.

4. Concluding remarks

Lithium ions were inserted and de-inserted in pelleted samples of perovskite-type oxides $Pr_{0.5+x-y}Li_{0.5-3x}Bi_y\square_{2x}TiO_3$. The amount of inserted lithium increases as both the number of vacancies increases and bismuth concentration decreases. Unit cell volume increases with insertion and then decreases upon de-insertion, but with some hysteresis. Thus, under the experimental conditions used, the insertion can be considered as reversible in terms of lithium content, but not in a structural sense. The resulting conductivity is directly correlated to the amount of inserted lithium and variations in the activation energy are also correlated.

The use of blocking electrodes and the Kramers–Kronig relations allowed the separation of the ionic and electronic conductivities. The starting and delithiated compositions are found to be purely

ionic conductors, while the lithiated compositions are found to be mixed conductors, although the ionic conductivity remains the dominant process. The ionic conductivity increases as more lithium is inserted due to the increase of the number of charge carriers. The activation energy of the ionic conductivity is inversely correlated to the unit cell volume, as the increase in cell volume reduces the influence of the bottleneck between A sites. The electronic conductivity is consistent with a polaron mechanism, with the conductivity increasing with the amount of inserted lithium resulting in an increase in the amount of Ti^{3+}. At the same time, the activation energy is almost constant (~0.8 eV), as it is only related to electron jumps from Ti^{3+} to Ti^{4+}.

Acknowledgments

We acknowledge the partial financial support for this work from projects MAT2007-63445 and 2005SGR00184, CONACyT-México, under projects 48970 and PAPIIT-UNAM under project IN-114406-2. M.F. García-Sánchez acknowledges the postdoctoral fellowship from ICyTDF-México DF under project PICCO 10-73. Partial support from University of Havana is gratefully acknowledged.

References

[1] Y. Inaguma, C. Liquan, M. Itoh, T. Nakamura, T. Uchida, H. Ikuta, M. Wakihara, Solid State Commun. 86 (1993) 689–693.
[2] H. Kawai, J. Kuwano, J. Electrochem. Soc. 141 (1994) L78–L79.
[3] G.-Y. Adachi, N. Imanaka, S. Tamura, Chem. Rev. 102 (2002) 2405–2429.
[4] E.A. Fortal'nova, O.N. Gavrilenkov, A.G. Belous, E.D. Politova, Russ. J. Gen. Chem. 79 (2009) 1987–1997.
[5] S. García-Martín, M.A. Alario-Franco, H. Ehrenberg, J. Rodríguez-Carvajal, U. Amador, J. Am. Chem. Soc. 126 (2004) 3587–3596.
[6] Y. Inaguma, T. Katsumata, M. Itoh, Y. Morii, T. Tsurui, Solid State Ionics 177 (2006) 3037–3044.
[7] R. Jimenez, A. Rivera, A. Varez, J. Sanz, Solid State Ionics 180 (2009) 1362–1371.
[8] P. Knauth, Solid State Ionics 180 (2009) 911–916.
[9] M.A. París, J. Sanz, C. León, J. Santamaría, J. Ibarra, A. Várez, Chem. Mater. 12 (2000) 1694–1701.
[10] A.I. Ruiz, M.L. López, M.L. Veiga, C. Pico, Solid State Ionics 112 (1998) 291–297.
[11] J. Sanz, A. Varez, J.A. Alonso, M.T. Fernandez, J. Solid State Chem. 177 (2004) 1157–1164.
[12] S. Stramare, V. Thangadurai, W. Weppner, Chem. Mater. 15 (2003) 3974–3990.
[13] A. Varez, J. Ibarra, A. Rivera, C. León, J. Santamaría, M.A. Laguna, M.L. Sanjuán, J. Sanz, Chem. Mater. 15 (2002) 225–232.
[14] S. García-Martin, F. García-Alvarado, A.D. Robertson, A.R. West, M.A. Alario-Franco, J. Solid State Chem. 128 (1997) 97–101.
[15] M.L. Sanjuán, M.A. Laguna, A.G. Belous, O.I. V'yunov, Chem. Mater. 17 (2005) 5862–5866.
[16] M. Morales, A.R. West, Solid State Ionics 91 (1996) 33–43.
[17] M. Catti, Chem. Mater. 19 (2007) 3963–3972.
[18] T. Katsumata, Y. Inaguma, M. Itoh, K. Kawamura, Chem. Mater. 14 (2002) 3930–3936.
[19] T. Onishi, Solid State Ionics 180 (2009) 592–597.
[20] A.R. Ruiz-Salvador, M.F. García-Sánchez, M. O'Reilly-Lukin, D.W. Lewis, A. Gómez, Phys. Status Solidi C 2 (2005) 3521–3524.
[21] M.F. García-Sánchez, N. Fernández, M.-L. Martínez-Sarrión, L. Mestres, M. Herraiz, P. Escribano, E. Cordoncillo, H. Beltrán, Phys. Status Solidi B 242 (2005) 1924–1927.
[22] M. Wagemaker, W.J.H. Borghols, F.M. Mulder, J. Am. Chem. Soc. 129 (2007) 4323–4327.
[23] P. Birke, S. Scharner, R.A. Huggins, W. Weppner, J. Electrochem. Soc. 144 (1997) L167–L169.
[24] O. Bohnke, C. Bohnke, J.L. Fourquet, Solid State Ionics 91 (1996) 21–31.
[25] C.H. Chen, K. Amine, Solid State Ionics 144 (2001) 51–57.
[26] J. Emery, O. Bohnke, J.L. Fourquet, J.Y. Buzare, P. Florian, D. Massiot, J. Phys.: Condens. Matter 11 (1999) 10401–10417.
[27] M.-L. Martínez-Sarrión, L. Mestres, M.R. Palacín, M. Herráiz, Eur. J. Inorg. Chem. (2001) 1139–1144.
[28] Y.-J. Shan, L. Chen, Y. Inaguma, M. Itoh, T. Nakamura, J. Power Sources 54 (1995) 397–402.
[29] Y.-J. Shan, Y. Inaguma, M. Itoh, Solid State Ionics 79 (1995) 245–251.
[30] O. V'yunov, O. Gavrilenko, L. Kovalenko, S. Chernukhin, L. Vasilechko, S. Kobilyanskaya, A. Belous, Russ. J. Inorg. Chem. 56 (2011) 93–98.
[31] M.F. García, N. Fernández, K. Borrego, M.-L. Martínez-Sarrión, L. Mestres, M. Herráiz, J. Eur. Ceram. Soc. 25 (2005) 729–734.
[32] M.-F. García-Sánchez, N. Fernández, M.-L. Martínez-Sarrion, L. Mestres, F. Fernández-Gutierrez, G. Santana, A.R. Ruiz-Salvador, Appl. Phys. Lett. 93 (2008) 034105.
[33] M.-L. Martínez-Sarrión, L. Mestres, M. Herráiz, O. Maqueda, N. Fernández, M.F. García, Eur. J. Inorg. Chem. (2003) 2458–2462.
[34] A.K. Jonscher, Dielectric Relaxation in Solids, Chelsea Dielectric Press, London, 1983.
[35] M.F. García-Sánchez, A. Ortiz, G. Santana, M. Bizarro, J. Peña, F. Cruz-Gandarilla, M.A. Aguilar-Frutis, J.C. Alonso, J. Am. Ceram. Soc. 93 (2010) 155–160.
[36] E. Barsoukov, J.R. Macdonald, Impedance Spectroscopy: Theory, Experiment and Applications, Wiley Interscience, New Jersey, 2005.
[37] M.T. Colomer, M. Maczka, J. Solid State Chem. 184 (2011) 365–372.
[38] O. Sánchez-Garrido, C. Gómez-Aleixandre, J.S. Olías, J.M. Albella, M. Hernández-Vélez, F. Fernández Gutiérrez, J. Mater. Sci.: Mater. Electron. 7 (1996) 297–303.
[39] M.F. García-Sánchez, J.-C. M'Peko, A.R. Ruiz-Salvador, G. Rodríguez-Gattorno, Y. Echevarría, F. Fernández-Gutierrez, A. Delgado, J. Chem. Educ. 80 (2003) 1062–1073.
[40] J. Jamnik, J. Maier, Phys. Chem. Chem. Phys. 3 (2001) 1668–1678.
[41] T. Talebi, M. Haji, B. Raissi, Int. J. Hydrogen Energy 35 (2010) 9420–9426.
[42] D.C. Cronemeyer, Phys. Rev. 113 (1959) 1222–1226.